

1 High-level cognition is supported by information-rich but
2 compressible brain activity patterns

3 Lucy L. W. Owen^{1,2} and Jeremy R. Manning^{1,*}

1^{Department of Psychological and Brain Sciences,}
Dartmouth College, Hanover, NH

2^{Carney Institute for Brain Sciences,}
Brown University, Providence, RI

*Address correspondence to jeremy.r.manning@dartmouth.edu

4 March 11, 2024

5 **Abstract**

6 Brain activity patterns are highly flexible and often complex, but also highly structured.
7 Here we examined how fundamental properties of brain activity patterns relate to ongoing
8 cognitive processes. To this end, we applied dimensionality reduction algorithms and pattern
9 classifiers to functional neuroimaging data collected as participants listened to a story, tem-
10 porally scrambled versions of the story, or underwent a resting state scanning session. These
11 experimental conditions were intended to require different depths of processing and inspire
12 different levels of cognitive engagement. We considered two primary aspects of the data. First,
13 we treated the maximum achievable decoding accuracy across participants as an indicator of
14 the “informativeness” of the recorded patterns. Second, we treated the number of features
15 (components) required to achieve a threshold decoding accuracy as a proxy for the “compress-
16 ability” of the neural patterns (where fewer components indicate greater compression). Overall,
17 we found that the peak decoding accuracy (achievable without restricting the numbers of fea-
18 tures) was highest in the intact (unscrambled) story listening condition. However, the number
19 of features required to achieve comparable classification accuracy was also lowest in the intact
20 story listening condition. Taken together, our work suggests that our brain networks flexibly
21 reconfigure according to ongoing task demands, and that the activity patterns associated with
22 higher-order cognition and high engagement are both more informative and more compressible
23 than the activity patterns associated with lower-order tasks and lower levels of engagement.

24 **Keywords:** information, compression, temporal decoding, dimensionality reduction, neu-
25 roimaging

26 **Significance Statement:** How our brains respond to ongoing experiences depends on what
27 we are doing and thinking about, among other factors. To study how brain activity reflects
28 ongoing cognition, we examined two fundamental aspects of brain activity under different cog-
29 nitive circumstances: informativeness and compressibility. Informativeness refers to the extent
30 to which brain patterns are both temporally specific and consistent across different people.
31 Compressibility refers to how robust the informativeness of brain patterns is to dimensionality
32 reduction. Brain activity evoked by higher-level cognitive tasks are both more informative
33 and more compressible than activity evoked by lower-level tasks. Our findings suggest that
34 our brains flexibly reconfigure themselves to optimize different aspects of how they function
35 according to ongoing cognitive demands.

36 Introduction

37 Large-scale networks, including the human brain, may be conceptualized as occupying one or
38 more positions along on a continuum. At one extreme, every node is fully independent from
39 every other node. At the other extreme, all nodes behave identically. Each extreme optimizes
40 key properties of how the network functions. When every node is independent, the network is
41 maximally *expressive*: if we define the network's "state" as the activity pattern across its nodes, then
42 every state is equally reachable by a network with fully independent nodes. On the other hand, a
43 network of identically behaved nodes optimizes *robustness*: any subset of nodes may be removed
44 from the network without any loss of function or expressive power, as long as any single node
45 remains. In addition to considering flexibility across space (nodes), these properties may also vary,
46 largely independently, across time. A network is maximally expressive when its nodes' activity
47 patterns vary in meaningful ways from moment to moment, whereas it is maximally robust to
48 signal corruption when its activity is constant over time. Presumably, most natural systems tend
49 to occupy positions between these temporal and spatial extremes. Under different circumstances,
50 it may even prove beneficial for systems to make different tradeoffs between expressiveness and
51 robustness along the temporal and spatial dimensions. We wondered: might the human brain
52 reconfigure itself to be more flexible or more robust according to ongoing demands? In other
53 words, might the brain reconfigure its connections or behaviors under different circumstances to
54 change its position along these continuums?

55 Closely related to the above notions of expressiveness versus robustness are measures of
56 how much *information* is contained in a given signal or pattern, and how *redundant* a signal
57 is (Shannon, 1948). Formally, information is defined as the amount of uncertainty about a given
58 variables' outcomes (i.e., entropy), measured in *bits*, or the optimal number of yes/no questions
59 needed to reduce uncertainty about the variable's outcomes to zero. Highly complex systems with
60 many degrees of freedom (i.e., high flexibility and expressiveness), are more information-rich than
61 simpler or more constrained systems. The redundancy of a signal denotes the difference between
62 how expressive the signal *could* be (i.e., proportional to the number of unique states or symbols
63 used to transmit the signal) and the actual information rate (i.e., the entropy of each individual
64 state or symbol). If a brain network's nodes are fully independent, then the number of bits required

65 to express a single activity pattern is proportional to the number of nodes. The network would
66 also be minimally redundant, since the status of every node would be needed to fully express a
67 single brain activity pattern. If a brain network's nodes are fully coupled and identical, then the
68 number of bits required to express a single activity pattern is proportional to the number of unique
69 states or values any individual node can take on. Such a network would be highly redundant,
70 since knowing any individual node's state would be sufficient to recover the full-brain activity
71 pattern. Highly redundant systems are also robust, since there is little total information loss due
72 to removing any given observation.

73 We take as a given that brain activity is highly flexible: our brains can exhibit nearly infinite
74 varieties of activity patterns. This flexibility implies that our brains' activity patterns are highly
75 information rich. However, brain activity patterns are also highly structured. For example,
76 full-brain correlation matrices are stable within (Finn et al., 2017, 2015; Gratton et al., 2018) and
77 across (Cole et al., 2014; Glerean et al., 2012; Gratton et al., 2018; Yeo et al., 2011) individuals. This
78 stability suggests that our brains' activity patterns are at least partially constrained, for example
79 by anatomical, external, or internal factors. Constraints on brain activity that limit its flexibility
80 decrease expressiveness (i.e., its information rate). However, constraints on brain activity also
81 increase its robustness to noise (e.g., "missing" or corrupted signals may be partially recovered).
82 For example, recent work has shown that full-brain activity patterns may be reliably recovered
83 from only a relatively small number of implanted electrodes (Owen et al., 2020; Scangos et al.,
84 2021). This robustness property suggests that the relevant signal (e.g., underlying factors that
85 have some influence over brain activity patterns) are compressible.

86 To the extent that brain activity patterns contain rich task-relevant information, we should be
87 able to use the activity patterns to accurately differentiate between different aspects of a task (e.g.,
88 using pattern classifiers; Norman et al., 2006). For example, prior work has shown a direct
89 correspondence between classification accuracy and the information content of a signal (Alvarez,
90 2002). To the extent that brain activity patterns are compressible, we should be able to generate
91 simplified (e.g., lower dimensional) representations of the data while still preserving the relevant
92 or important aspects of the original signal. In general, information content and compressibility
93 are often related but are also dissociable (Fig. 1). If a given signal (e.g., a representation of brain
94 activity patterns) contains more information about ongoing cognitive processes, then the peak

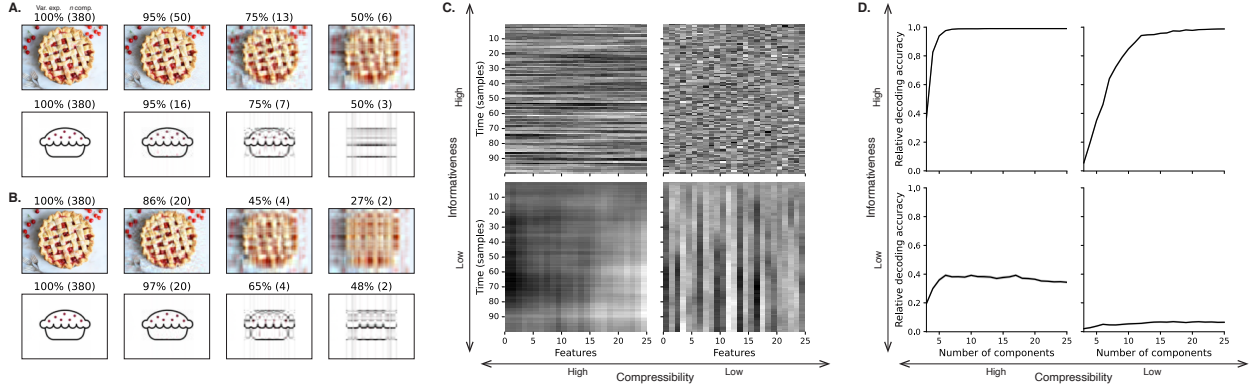


Figure 1: Information content and compressibility. **A. Variance explained for two images.** Consider two example images: a photograph and simple drawing. The images have the same resolutions, but their content is very different. The photograph is more information rich: when we compare the original photograph and drawing (leftmost column), we can see that the photograph captures much more detail. We can also apply principal components analysis to the images, treating the rows of the images as “observations.” Across columns, we identified the numbers of components required to explain 100%, 95%, 75%, or 50% of the cumulative variance in each image (the 100% columns denote the original images). The numbers of components are indicated in parentheses, and the resulting “compressed” images are displayed. This analysis reveals that the drawing is more compressible: just 16 components can explain 95% of the variance in the drawing, whereas 50 components are required to explain 95% of the variance in the photograph. **B. Representing two images with different numbers of components.** Using the same principal component decompositions as in Panel A, we computed the cumulative proportion of variance explained with 380 (original images), 20, 4, or 2 components. This analysis provides another way of characterizing the compressibility of each image by showing that the same number of components can explain more variance in the drawing than in the photograph. **C. Template data from four synthetic datasets.** We constructed four synthetic datasets, each comprising 25 features (columns) observed across 100 samples (rows) from each of 10 simulated “participants.” The datasets were constructed to contain different levels of informativeness and compressibility (see *Synthetic data*). **D. Decoding accuracy by number of components.** For each synthetic dataset, we trained across-participant classifiers to decode timepoint labels. Each panel displays the decoding accuracy as a function of the number of components used to represent the data. Error ribbons denote bootstrap-estimated 95% confidence intervals.

95 decoding accuracy should be high. In the simulations shown in Figure 1C we construct synthetic
96 datasets that have high or low levels of informativeness by varying temporal autocorrelations
97 in the data (see *Synthetic data*). If a signal is compressible, then a low-dimensional embedding
98 of the signal will be similarly informative as the original signal. In the simulations shown in
99 Figure 1C we construct synthetic datasets that have high or low levels of compressibility by
100 varying the covariance structure across features (see *Synthetic data*). As shown in Figure 1D, highly
101 informative datasets yield higher decoding accuracies than less informative datasets (i.e., the peaks
102 of the curves in the top panels of Fig. 1D are higher than the peaks of the curves in the bottom
103 panels). Highly compressible datasets show steeper slopes when we plot decoding accuracy as a
104 function of the number of components used to represent the data (i.e., the slopes of the curves in
105 the left panels of Fig. 1D are steeper than the slopes of the curves in the right panels). Whereas
106 characterizing the informativeness and compressibility of synthetic data can be instructive, we
107 are ultimately interested in understanding how these properties relate to brain activity patterns
108 recorded under different cognitive circumstances.

109 Several recent studies suggest that the complexity of brain activity is task-dependent, whereby
110 simpler tasks with lower cognitive demands are reflected by simpler and more compressible brain
111 activity patterns, and more complex tasks with higher cognitive demands are reflected by more
112 complex and less compressible brain activity patterns (Mack et al., 2020; Owen et al., 2021). These
113 patterns hold even when the stimulus itself is held constant (Mack et al., 2020). These findings
114 complement other work suggesting that functional connectivity (correlation) patterns are task-
115 dependent (Cole et al., 2014; Finn et al., 2017; Owen et al., 2020), although see Gratton et al. (2018).
116 Higher-order cognitive processing of a common stimulus also appears to drive more stereotyped
117 task-related activity and functional connectivity across individuals (Hasson et al., 2008; Lerner et
118 al., 2011; Simony & Chang, 2020; Simony et al., 2016).

119 The above studies are consistent with two potential descriptions of how cognitive processes are
120 reflected in brain activity patterns. One possibility is that the information rate of brain activity in-
121 creases during more complex or higher-level cognitive processing. If so, then the ability to reliably
122 decode cognitive states from brain activity patterns should improve with task complexity or with
123 the level (or “depth”) of cognitive processing. A second possibility is that the compressibility of
124 brain activity patterns decreases during more complex or higher-level cognitive processing. If so,

125 then individual features of brain recordings should carry more information (over and above the
126 information carried by other features) during complex or high-level (versus simple or low-level)
127 cognitive tasks. The tradeoffs between these two aspects of brain activity may also vary across
128 brain regions or networks, for example according to each region's functional role.

129 We used a previously collected neuroimaging dataset to estimate the extent to which each of
130 these two possibilities might hold. The dataset we examined comprised functional magnetic res-
131 onance imaging (fMRI) data collected as participants listened to an audio recording of a 7-minute
132 story, temporally scrambled recordings of the story, or underwent a resting state scan (Simony
133 et al., 2016). Each of these experimental conditions evokes different depths of cognitive process-
134 ing (Hasson et al., 2008; Lerner et al., 2011; Owen et al., 2021; Simony et al., 2016). We used
135 across-participant classifiers to decode listening times in each condition, as a proxy for how "infor-
136 mative" the task-specific activity patterns were (Simony & Chang, 2020). We also used principle
137 components analysis to generate lower-dimensional representations of the activity patterns. We
138 then repeated the classification analyses after preserving different numbers of components and
139 examined how classification accuracy changed across the different experimental conditions.

140 Results

141 We sought to understand whether higher-level cognition is reflected by more reliable and in-
142 formative brain activity patterns, and how compressibility of brain activity patterns relates to
143 cognitive complexity. We developed a computational framework for systematically assessing the
144 informativeness and compressibility of brain activity patterns recorded under different cognitive
145 circumstances. We used across-participant decoding accuracy (see *Forward inference and decoding*
146 *accuracy*) as a proxy for informativeness. To estimate the compressibility of the brain patterns, we
147 used group principal components analysis (PCA) to project the brain patterns into k -dimensional
148 spaces, for different values of k (see *Hierarchical Topographic Factor Analysis (HTFA)* and *Principal*
149 *components analysis (PCA)*). For more compressible brain patterns, decoding accuracy should be
150 more robust to small values of k .

151 We analyzed a dataset collected by Simony et al. (2016) that comprised four experimental con-
152 ditions. These conditions exposed participants to stimuli that systematically varied in cognitive

engagement. In the *intact* experimental condition, participants listened to an audio recording of a 7-minute Moth Radio Hour story, *Pie Man*, by Jim O’Grady. In the *paragraph*-scrambled experimental condition, participants listened to a temporally scrambled version of the story, where the paragraphs occurred out of order, but where the same set of paragraphs was presented over the entire listening interval. All participants in this condition experienced the scrambled paragraphs in the same order. In the *word*-scrambled experimental condition, participants listened to a temporally scrambled version of the story, where the words occurred in a random order. Again, all participants in this condition experienced the scrambled words in the same order. Finally, in the *rest* experimental condition, participants lay in the scanner with no overt stimulus, while keeping their eyes open and blinking as needed. This public dataset provided a convenient means for testing our hypothesis that different levels of cognitive processing and engagement affect how informative and compressible the associated brain patterns are.

To evaluate the relation between informativeness and compressibility for brain activity from each experimental condition, we trained a series of across-participant temporal decoders on compressed representations of the data. Figure 2A displays the decoding accuracy as a function of the number of principal components used to represent the data (also see Fig. S2). Several patterns were revealed by the analysis. First, in general (i.e., across experimental conditions), decoding accuracy tends to improve as the number of components are increased. However, decoding accuracy peaked at higher levels for experimental conditions that exposed participants to cognitively richer stimuli (Fig. 2D). The peak decoding accuracy was highest for the “intact” condition (versus paragraph: $t(99) = 35.205, p < 0.001$; versus word: $t(99) = 43.172, p < 0.001$; versus rest: $t(99) = 81.361, p < 0.001$), next highest for the “paragraph” condition (versus word: $t(99) = 6.243, p < 0.001$; versus rest: $t(99) = 50.748, p < 0.001$), and next highest for the “word” condition (versus rest: $t(99) = 48.791, p < 0.001$). This ordering implies that cognitively richer conditions evoke more stable brain activity patterns across people.

The cognitively richer conditions also displayed steeper initial slopes. For example, the intact condition decoders reached an arbitrarily chosen threshold of 5% accuracy using fewer components than the paragraph condition decoders ($t(99) = -7.429, p < 0.001$) or word condition decoders ($t(99) = -7.300, p < 0.001$), and decoding accuracy never exceeded 5% for the rest condition. This suggests that brain activity patterns evoked by cognitively richer conditions are more compressible,

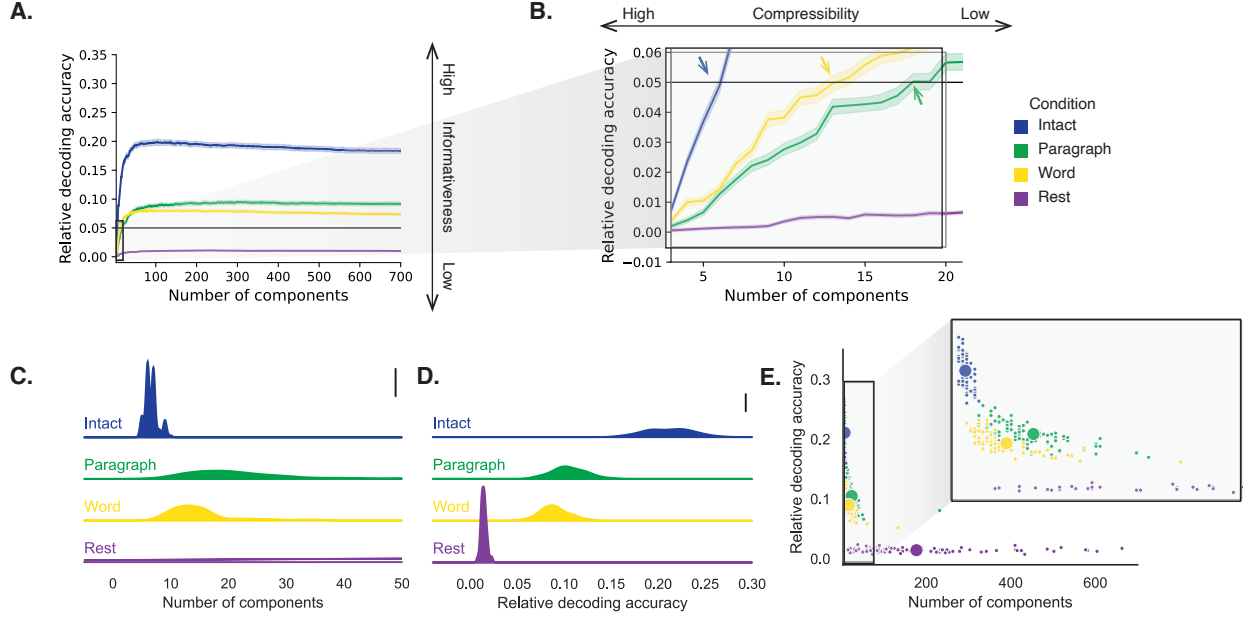


Figure 2: Decoding accuracy and compression. **A. Decoding accuracy by number of components.** Ribbons of each color display cross-validated decoding performance for each condition (intact, paragraph, word, and rest), as a function of the number of components (features) used to represent the data. For each condition, decoding accuracy has been normalized by subtracting expected “chance” decoding performance (estimated as $\frac{1}{T}$, where T is the number of timepoints in the given condition). This normalization was intended to enable fairer comparisons across conditions; a relative decoding accuracy of 0.0 denotes “chance” performance. The horizontal black line denotes 5% decoding accuracy (used as a reference in Panel B). **B. Numbers of components required to reach a fixed decoding accuracy threshold, by condition.** The panel displays a zoomed-in view of the inset in Panel A. Intersections between each condition’s decoding accuracy curve and the 5% decoding accuracy reference line are marked by arrows. All error ribbons in Panels A and B denote bootstrap-estimated 95% confidence intervals. **C. Estimating “compressibility” for each condition.** The probability density plots display the numbers of components required to reach at least 5% (corrected) decoding accuracy, across all cross validation runs. For the “rest” condition, where decoding accuracy never reached 5% accuracy, we display the distribution of the numbers of components required to achieve the peak decoding accuracy in each fold. (This distribution is nearly flat, as also illustrated in Panel E.) The scale bar denotes a height of 0.01. **D. Estimating “informativeness” for each condition.** The probability density plots display the peak (corrected) decoding accuracies achieved in each condition, across all cross validation runs. The scale bar denotes a height of 0.01. **E. Informativeness versus compressibility.** Each dot displays the minimum number of components required to achieve at least 5% corrected decoding accuracy (x -coordinate; for the rest condition the numbers of components are estimated using the peak decoding accuracies as in Panel C) and the peak (corrected) decoding accuracy (y -coordinate). The smaller dots correspond to individual cross validation runs and the larger dots display the averages across runs. The inset displays a zoomed-in view of the indicated region in the main panel.

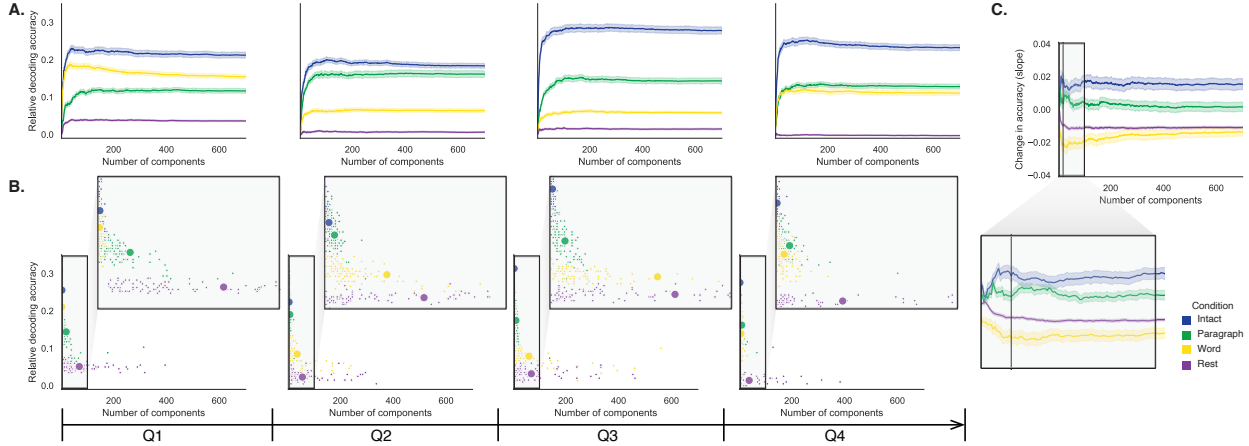


Figure 3: Changes in decoding accuracy and compression over time. **A. Decoding accuracy by number of components, by story segment.** Each family of curves is plotted in the same format as Figure 2A but reflects data only from one quarter of the dataset. **B. Informativeness versus compressibility by condition and segment.** Each scatter plot is in the same format as Figure 2E, but reflects data only from one quarter of the dataset. **C. Change in decoding accuracy over time, by number of components.** For each number of components (x -axis) and condition (color), we fit a regression line to the decoding accuracies obtained for the first, second, third, and fourth quarters of the dataset (corresponding to the columns of Panels A and B). The y -axis denotes the slopes of the regression lines. The black vertical line marks $k = 20$ components, as referenced in the main text. All error ribbons denote bootstrap-estimated 95% confidence intervals.

such that representing the data using the same number of principal components provides more information to the temporal decoders (Figs. 2B, C). Taken together, as shown in Figure 2E, we found that brain activity patterns evoked by cognitively richer conditions tended to be both more informative (i.e., associated with higher peak decoding accuracies) *and* more compressible (i.e., requiring fewer components to achieve the 5% accuracy threshold).

If informativeness (to the temporal decoders) and compressibility vary with the cognitive richness of the stimulus, might these measures also vary over time *within* a given condition? For example, participants in the intact condition might process the ongoing story more deeply later on in the story (compared with earlier in the story) given the additional narrative background and context they had been exposed to by that point. To examine this possibility, we divided each condition into four successive time segments. We computed decoding curves (Fig. 3A) and the numbers of components required to achieve 5% decoding accuracy (Fig. 3B) for each segment and condition. We found that, in the two most cognitively rich conditions (intact and paragraph), both decoding accuracy and compressibility, as reflected by the change in decoding curves, increased

197 with listening time (e.g., at the annotated reference point of $k = 20$ components in Fig. 3C: intact:
198 $t(99) = 7.915, p < 0.001$; paragraph: $t(99) = 2.354, p = 0.021$). These changes may reflect an increase
199 in comprehension or depth of processing with listening time. In contrast, the decoding accuracy
200 and compressibility *decreased* with listening time in the word condition ($t(99) = -10.747, p < 0.001$)
201 and rest condition ($t(99) = -22.081, p < 0.001$). This might reflect the depletion of attentional
202 resources in the less-engaging word and rest conditions.

203 These results make some intuitive sense. As the contextual information available to participants
204 increases (i.e., over time in the cognitively rich intact and paragraph conditions), it makes sense that
205 this might constrain neural responses to a greater extent. While this pattern may not necessarily
206 hold for *every* possible story or stimulus, we suspect that it is generally the case that our knowledge
207 about what is happening in a story tends to increase as we experience more of it. In turn, this
208 could lead to greater consistency in different people's interpretations of and neural responses to
209 the stimulus. Similarly, as participants are left to "mind wander," or as they experience mental
210 fatigue (i.e., over time in the less cognitively rich word and rest conditions), we suggest that this
211 might lead to greater variability in neural responses across people, resulting in lower decoding
212 accuracy. Again, it is not necessarily the case that every possible "unengaging" stimulus will
213 lead to greater neural variability as time progresses, but we suspect this phenomenon is likely to
214 hold for a variety of such stimuli. These findings replicate at least to a limited extent (e.g., across
215 both cognitively rich conditions and across both cognitively impoverished conditions, and for the
216 different groups of participants in each of those conditions). However, determining whether these
217 patterns generalize to other stimuli would require additional study (with new stimuli).

218 If the informativeness and compressibility of brain activity patterns vary over time, might these
219 properties also vary across brain networks? We used a network parcellation identified by Yeo et
220 al. (2011) to segment the brain into seven distinct networks. The networks can be sorted (roughly)
221 in order from lower-level to higher-level cortex as follows (Figs. 4A–C): visual, somatomotor,
222 dorsal attention, ventral attention, limbic, frontoparietal, and default mode. Next, we computed
223 decoding curves separately for the activity patterns within each network and identified each
224 network's inflection point, for each experimental condition. Moving from low-order networks
225 to higher-order networks, we found that decoding accuracy tended to increase in the higher-
226 level experimental conditions and decrease (slightly) in the lower-level experimental conditions

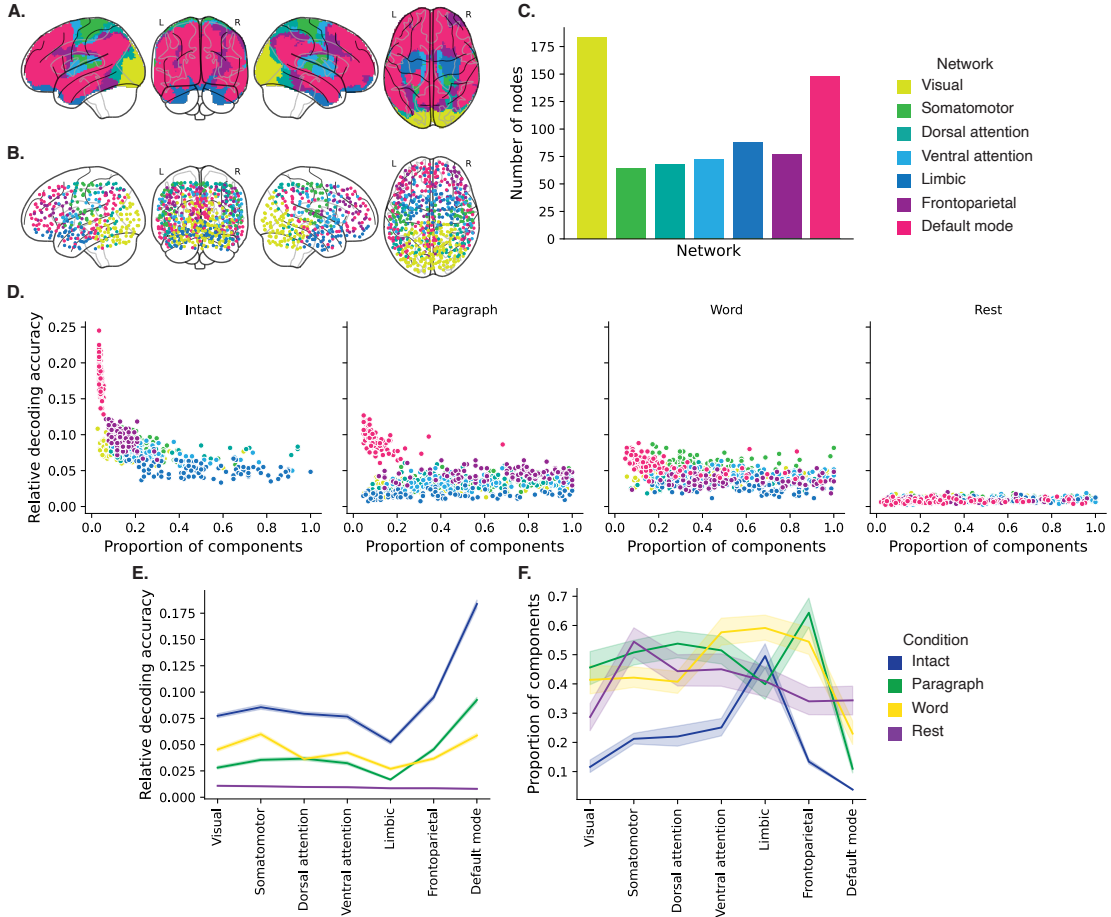


Figure 4: Network-specific decoding accuracy and compression. **A. Network parcellation map.** The glass brain displays the location of each of seven networks identified by Yeo et al. (2011). **B. Node labels.** We assigned network labels to each of 700 Hierarchical Topographic Factor Analysis-derived nodes (see *Hierarchical topographic factor analysis (HTFA)*). For each node, we evaluated its radial basis function (RBF) at the locations of every voxel in the parcellation map displayed in Panel A. We summed up these RBF weights separately for the voxels in each network. We defined each node's network label as its highest-weighted network across all voxels. **C. Per-network node counts.** The bar plot displays the total number of HTFA-derived nodes assigned to each network. **D. Informativeness versus compressibility by network and condition.** Each dot corresponds to a single cross validation run. The dots' coordinates denote the minimum proportion of components (relative to the number of nodes in the given network) required to achieve at least 5% corrected decoding accuracy (x -coordinate; for the rest condition these proportions are estimated using the peak decoding accuracies) and peak (corrected) decoding accuracy (y -coordinate). We repeated the analysis separately for each network (color) and experimental condition (column). **E. Informativeness by network.** For each network, sorted (roughly) from lower-order networks on the left to higher-order networks on the right, the curves display the peak (corrected) decoding accuracy for each experimental condition (color). **F. Compressibility by network.** For each network, the curves display the proportion of components (relative to the total possible number of components displayed in Panel C) required to achieve at least 5% decoding accuracy (or, for the rest condition, peak decoding accuracy, as described above). Error ribbons in Panels E and F denote bootstrap-estimated 95% confidence intervals.

(Fig. 4D, E; Spearman's rank correlation between decoding accuracy and network order: intact: $\rho = 0.362, p < 0.001$; paragraph: $\rho = 0.441, p < 0.001$; word: $\rho = -0.102, p = 0.007$; rest: $\rho = -0.354, p < 0.001$). This suggests that higher-order networks may carry more content-relevant or stimulus-driven "information." We found no clear trends in the proportions of components required to achieve 5% decoding accuracy across networks or conditions (Fig. 4F). We note that the limbic network we considered here often overlaps with low (imaging) signal regions, and therefore it may be difficult to draw strong conclusions about this network's informativeness or compressibility. We also considered the possibility that the correlations with network order might be influenced by the numbers of nodes in each network. We designed a permutation-based procedure to address this possibility, whereby we repeated the above analyses using shuffled network labels (see *Network permutation tests*). The correlations between decoding accuracy and network order were reliably more positive than the shuffled correlations for the intact ($t(1998) = 276.431, p < 0.001$) and paragraph ($t(1998) = 330.334, p < 0.001$) conditions, and reliably more negative for the word ($t(1998) = -16.386, p < 0.001$) and rest ($t(1998) = -318.631, p < 0.001$) conditions. These results suggest that the correlations between decoding accuracy and network order were not driven solely by the numbers of nodes in each network.

Whereas the above analyses examined different networks in isolation, how does full-brain (i.e., potentially multi-network) activity patterns reflected by different principal components vary across different experimental conditions? As shown in Figure 5, we used Neurosynth (Rubin et al., 2017) to identify, for each component, the associations with each of 80 themes (see *Reverse inference*). In general, the first principal components across all of the experimental conditions tended to weigh most heavily on themes related to cognitive control, memory, language processing, attention, and perception. Other components appeared to vary more across conditions.

To gain further insights into which brain functions might be most closely associated with the top-weighted components from each experimental condition, we manually grouped each Neurosynth-derived topic into a smaller set of core cognitive functions. Separately for each component, we computed the average weightings across all topics that were tagged as being associated with each of these cognitive functions (Figs. 6A, S6A). To help visualize these associations, we used the patterns of associations for each component to construct graphs whose nodes were experimental conditions and cognitive functions (Figs. 6B, S6B). We also computed correlations between the

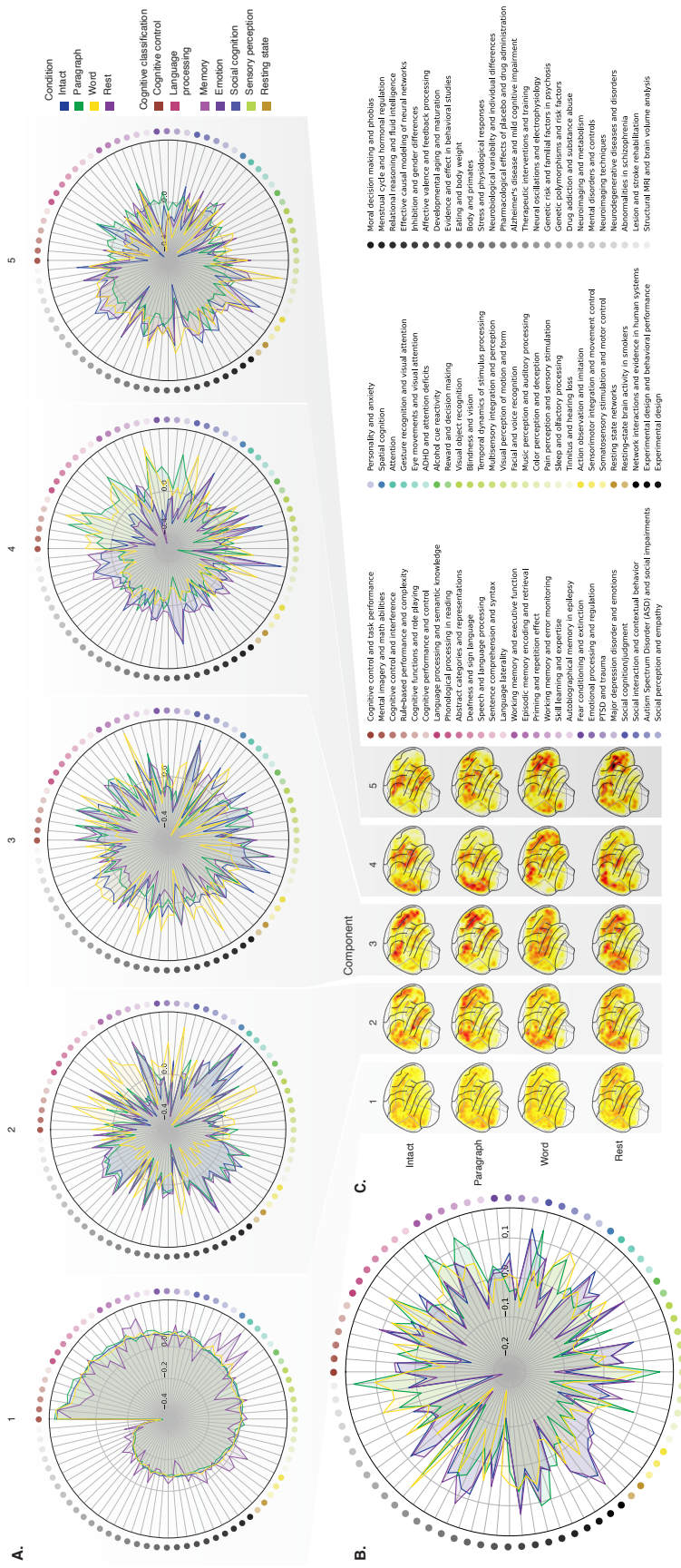


Figure 5: Neurosynth topic weightings by component. We used a reverse inference procedure (see *Reverse inference*) to estimate the correspondences between brain images and a set of 80 topics derived from the Neurosynth database of neuroimaging articles (Rubin et al., 2017). **A. Topic correlations by component.** For each of the top five highest-weighted principal components (columns) derived from each experimental condition (colors), the radar plots display the correlations between the component images and the per-topic images derived for each topic (topic identities are denoted by the blue dots; a legend for the topic labels is in the lower right of the figure). An annotated list of the top-weighted topics for each component and condition may be found in Figure S3 and the top-weighted terms for each topic may be found in Table S1. **B. Topic correlations averaged across components.** The radar plot is in the same format as the plots in Panel A, but here we display the per-condition average correlations across the top five components (for each condition) reflected in Panel A. **C. Component images.** Each plot displays a right sagittal view of a glass brain projection of the top five principal components (columns) for each experimental condition (rows). Additional projections for each component may be found in Figure S4.

sets of per-topic weightings from each of the top-weighted components from each experimental condition (Fig. 6C, D) and between the brain maps for each condition's components (Fig. S6C, D). Taken together, we found that each component appeared to weigh on a fundamental set of cognitive functions that varied by experimental condition. For example, the top principal components from every condition weighed similarly (across conditions) on the full set of Neurosynth topics (Fig. 5A) and cognitive functions (Figs. 6A, B and S6 A, B), suggesting that these components might reflect a set of functions or activity patterns that are common across all conditions. The second components' weightings were similar across the intact, paragraph, and rest conditions (highest-weighted functions: cognitive control, memory, social cognition, and resting state), but different for the word condition (highest-weighted functions: sensory perception and cognitive control). The fourth components' weighting grouped the paragraph and word conditions (highest-weighted functions: memory, language processing, and cognitive control) and the intact and rest conditions (highest-weighted functions: emotion, social cognition). We also used ChatGPT (OpenAI, 2023) to sort the list of manually tagged cognitive functions from lowest-level to highest-level (Tab. S2, Fig. 6E; also see *Ranking cognitive processes*). We found that higher-level functions tended to be weighted more heavily by top components from the intact and paragraph conditions than lower-level functions (intact vs. word: $t(198) = 11.059, p < 0.001$; intact vs. rest: $t(198) = 3.699, p < 0.001$; paragraph vs. word: $t(198) = 13.504, p < 0.001$; paragraph vs. rest: $t(198) = 4.812, p < 0.001$; also see *Ranking cognitive processes*). The top components from the word condition showed the opposite tendency, whereby *lower*-level functions tended to be weighted more heavily than higher-level functions (word vs. rest: $t(198) = -7.315, p < 0.001$). The weighting trends for the intact and paragraph conditions were not reliably different ($t(198) = -0.479, p = 0.633$). The components from the rest condition showed only a small trending difference in the weights associated with high-level versus low-level functions (rest vs. 0: $t(99) = 1.836, p = 0.081$). These findings suggest that when participants were engaged more strongly (in the more engaging intact and paragraph conditions), their dominant neural patterns reflected higher-level cognitive functions. In contrast, when participants were engaged less strongly (in the less engaging word and rest conditions), their dominant neural patterns reflected lower-level cognitive functions. Although they were highly statistically reliable, it is also important to note that these latter effects are also relatively small (e.g., the slopes for *all* of the experimental conditions are numerically close to zero; Fig. 6E). We suggest

287 that this phenomenon may merit further investigation in future work.

288 Discussion

289 We examined fMRI data collected as participants listened to an auditory recording of a story,
290 scrambled recordings of the story, or underwent a resting state scan. We found that cognitively
291 richer stimuli evoked more reliable (i.e., consistent across people) and information rich brain activ-
292 ity patterns. The brain patterns evoked by cognitively richer stimuli were also more compressible,
293 in that each individual component provided more “signal” to temporal decoders relative to com-
294 ponents of data from less cognitively rich conditions (Fig. 2). Over time (e.g., as the experiment
295 progressed), these phenomena were strengthened. Specifically, across story segments, data from
296 more cognitively rich conditions became more informative and compressible, and data from less
297 cognitively rich conditions became *less* informative and compressible (Fig. 3). We also repeated
298 these analyses separately for different brain networks. We found that networks traditionally as-
299 sociated with higher-level cognitive functions tended to provide more informative brain patterns
300 than networks traditionally associated with lower level cognitive functions (Fig. 4). Finally, we
301 examined the most dominant components of the brain activity patterns from each experimental
302 condition. We used a reverse inference approach (Rubin et al., 2017) to identify the terms in the
303 neuroimaging literature most commonly associated with the corresponding maps. As summarized
304 in Figure 6E, we found that the intact and paragraph conditions tended to weight higher-level cog-
305 nitive processes more than lower-level cognitive processes, whereas the word condition weighted
306 lower-level processes more than higher-level processes and the rest condition showed no reliable
307 difference in high-level versus low-level weightings. Taken together, our findings indicate that the
308 informativeness and compressibility of our brain activity patterns are task-dependent, and these
309 properties change systematically with factors like cognitive richness and depth of processing.

310 Our explorations of informativeness and compressibility are related to a much broader litera-
311 ture on the correlational and causal structure of brain activity patterns and networks (Adachi et
312 al., 2012; Bassett & Sporns, 2017; Brovelli et al., 2004; Bullmore & Sporns, 2009; Dhamala et al.,
313 2008; Korzeniewska et al., 2008; Lynn & Bassett, 2021; Owen et al., 2021; Preti et al., 2017; Rogers
314 et al., 2007; Rubinov & Sporns, 2010; Sizemore et al., 2018; Smith, Beckmann, et al., 2013; Smith,

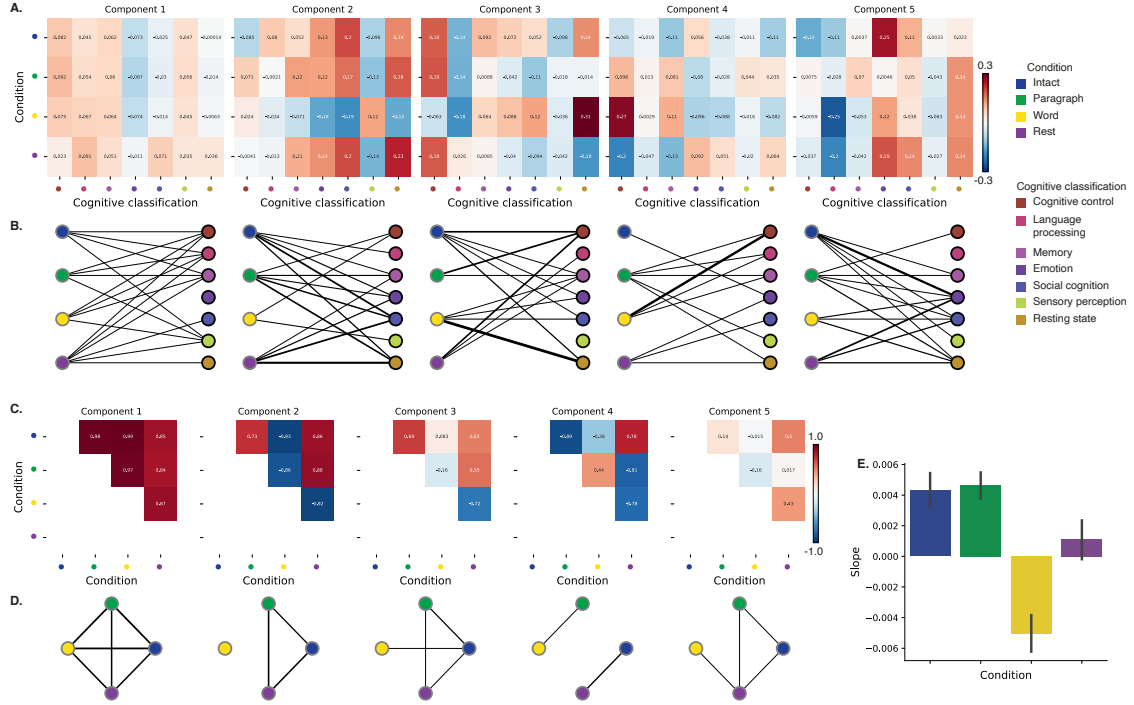


Figure 6: Summary of functions associated with top-weighted components by condition. **A. Top-weighted topics by condition.** Here we display per-condition (rows, indicated by colored dots) topic correlations, averaged across topics that pertain to each of several broad cognitive functions (columns within each sub-panel, indicated by colored dots). Each sub-panel reflects correlations for the components indicated in the panel titles. Table S1 provides a list of each topic’s top-weighted terms, along with each topic’s manually labeled cognitive classification. A full list of the topics most highly associated with each component may be found in Figure S3. **B. Associations between per-condition components and cognitive functions.** The network plots denote positive average correlations between the component images for each condition (gray-outlined dots on the left sides of each network; colors denote conditions) and topic-specific brain maps associated with each indicated cognitive function (black-outlined dots on the right sides of each network; colors denote cognitive functions). The line thicknesses are proportional to the correlation values (correlation coefficients are noted in the heat maps in Panel A). **C. Correlations between each principal component, by condition.** The heat maps display the correlations between the brain maps (Fig. S4) for each principal component (sub-panel), across each pair of conditions (rows and columns of each sub-panel’s matrix, indicated by colored dots). **D. Associations between per-condition components, by component.** Each sub-panel’s network plot summarizes the pattern of correlations between the n^{th} top-weighted principal components (sub-panel) for each experimental condition (gray-outlined dots). The line thicknesses are proportional to the correlation values (correlation coefficients are noted in the heat maps in Panel C). **E. Change in weights by condition.** The bar heights reflect the slopes of regression lines, fit separately to the top five components from each condition, between the ChatGPT-derived “rank” of each cognitive classification and the correlations between the component and topic maps associated with cognitive processes at the given rank (see *Ranking cognitive processes*) Error bars denote bootstrap-estimated 95% confidence intervals. Also see Fig. S6 for additional information.

315 Vidaurre, et al., 2013; Sporns & Betzel, 2016; Sporns & Honey, 2006; Sporns & Zwi, 2004; Srinivasan
316 et al., 2007; Tomasi & Volkow, 2011; Yeo et al., 2011; ?). Correlations or causal associations between
317 different brain regions simultaneously imply that full-brain activity patterns will be compressible
318 and also that those activity patterns will contain redundancies. For example, the extent to which
319 activity patterns at one brain area can be inferred or predicted from activity patterns at other
320 areas (e.g., Owen et al., 2020; Scangos et al., 2021), reflects overlap in the information available
321 in or represented by those brain areas. If brain patterns in one area are recoverable using brain
322 patterns in another area, then a “signal” used to convey the activity patterns could be compressed
323 by removing the recoverable activity. Predictable (and therefore redundant) brain activity patterns
324 are also more robust to signal corruption. For example, even if the activity patterns at one region
325 are unreadable or unreliable at a given moment, that unreliability could be compensated for by
326 other regions’ activity patterns that were predictive of the unreliable region. Whereas compressible
327 brain patterns are robust to spatial signal corruption, high versus low informativeness reflects a
328 similar (though dissociable; e.g., Fig. 1) tradeoff between expressiveness and robustness of *tempo-*
329 *ral* patterns. Highly informative brain patterns (by our measure; i.e., patterns that yield greater
330 temporal decoding accuracy) are expressive about ongoing experiences or cognitive states, since
331 each moment’s pattern is reliably distinguishable from other moments’ patterns. However, when
332 each moment’s pattern is unique, brain activity becomes less robust to temporal signal corruption.
333 Our finding that brain activity patterns becomes more informative (i.e., less robust to temporal
334 signal corruption) and compressible (i.e., more robust to spatial signal corruption) when cognitive
335 engagement is higher suggests that our brain may optimize its activity patterns to prioritize either
336 temporal or spatial robustness, according to task demands.

337 Our findings that informativeness and compressibility change with task demands may follow
338 from task-dependent changes in full-brain correlation patterns. A number of prior studies have
339 found that so-called “functional connectivity” (i.e., correlational) patterns vary reliably across
340 tasks, events, and situations (Cole et al., 2014; Owen et al., 2021; Simony et al., 2016; Smith et
341 al., 2009). By examining how these task-dependent changes in correlations affect informativeness
342 and compressibility, our work suggests a potential reason why the statistical structure of brain
343 activity patterns might vary with cognitive task or with cognitive demands. For lower-level tasks,
344 or for tasks that require relatively little “deep” cognitive processing, our brains may optimize

345 activity patterns for robustness and redundancy over expressiveness, for example to maximize
346 reliability. For higher-level tasks, or for tasks that require deeper cognitive processing, our brains
347 may sacrifice some redundancy in favor of greater expressiveness.

348 One potential limitation of our work concerns how our measure of informativeness might gen-
349 eralize across different tasks, cognitive representations, and processes. As in many neuroimaging
350 studies, our findings may also be influenced by our preprocessing decisions, which could in turn
351 affect temporal and spatial correlations in the data. Our use of across-participant temporal decod-
352 ing accuracy as a proxy for informativeness is motivated in part by prior work that introduced
353 across-participant similarity (in time-varying response to a stimulus) as a means of identifying
354 stimulus-driven brain activity patterns (Simony et al., 2016). Intuitively, only activity patterns that
355 are driven by the stimulus would be expected to synchronize (i.e., be time-locked to the stimulus)
356 across participants. This approach implicitly removes idiosyncratic responses (e.g., neural patterns
357 that are *not* similar across people). However, there are also some published examples, including
358 in our own prior work, that indicate that some types of stimulus-evoked activity will be missed by
359 across-participant comparisons. For example we have reported how brain regions like the ventro-
360 medial prefrontal cortex (vmPFC) show stimulus-driven responses that are, for the most part, *not*
361 similar across people (Chang et al., 2021). In that paper (and drawing on other work), we suggest
362 that the vmPFC seems to represent or support highly idiosyncratic internal states, like affective
363 responses. Although we would consider the vmPFC to be a “high-level” region (e.g., we consider
364 affect to be a relatively high-level aspect of cognition), the measure of informativeness that we
365 used in our current study would identify regions like the vmPFC as having *low* informativeness.
366 This is because across-participant decoding accuracy (our proxy measure for informativeness) will
367 only be high for representations or responses that are common across people.

368 Relatedly, even in the experimental conditions we describe as “less cognitively engaging,” we
369 think it likely that high-level thought or cognitive processing is still present. Rather, we suggest
370 that these high-level representations will tend to be more idiosyncratic when the stimulus is less
371 engaging, and therefore less constraining on people’s thoughts. Nonetheless, even during highly
372 engaging tasks, people may engage in idiosyncratic stimulus-driven processes. For example, peo-
373 ple might retrieve personal information as they listened to the story. Those retrievals could happen
374 at different times for different people according to each individual’s prior experiences. Even when

375 those sorts of retrievals happen to be temporally synchronized across people, the specific memo-
376 ries or information being retrieved might still be idiosyncratic. Our measure of informativeness
377 is insensitive to these processes. Further, even in response to an identical stimulus, task instruc-
378 tions or participants' internal goals could change the relationship between compressibility and
379 informativeness. Some work has shown that the "dimensionality" of neural representations can
380 change systematically with task complexity, even in response to an identical stimulus (Mack et al.,
381 2020). Taken together, we expect that the way we have defined informativeness in this paper, and
382 the specific dataset we examined, are likely to have influenced our findings. While we see our
383 approach as a reasonable first step, we also suggest that future work should explore alternative
384 measures of informativeness and compressibility, and should examine how these measures vary
385 across different tasks and datasets.

386 In the information theory sense (Shannon, 1948), when a signal is transmitted using a fixed
387 alphabet of "symbols," the information rate decreases as the signal is compressed (e.g., fewer sym-
388 bols transmitted per unit time, using an alphabet with fewer symbols, etc.). Our finding that each
389 individual brain component (symbol) becomes more informative as cognitive richness increases
390 suggests that the "alphabet" of brain activity patterns is also task-dependent. Other work suggests
391 that the representations that are *reflected* by brain activity patterns may also change with task de-
392 mands. For example, our brains may represent the same perceptual stimulus differently depending
393 on which aspects of the stimulus or which combinations of features are task-relevant (Mack et al.,
394 2020).

395 We found that different brain networks varied in how informative and compressible their
396 activity patterns were across experimental conditions (e.g., Fig. 4). This might follow from evolu-
397 tionary optimizations that reflect the relevant constraints or demands placed on those networks.
398 One possibility is that cortex is organized in a hierarchy of networks "concerned with" or selective
399 to different levels of processing or function. To the extent that different levels of processing (e.g.,
400 low-level sensory processing versus "deeper" higher-level processing) reflect different stimulus
401 timescales (e.g., Manning, 2023), the network differences we observed might also relate to the
402 timescales at which each network is maximally sensitive (Baldassano et al., 2017; Hasson et al.,
403 2008; Lerner et al., 2011; Regev et al., 2018).

404 Our reverse inference analyses (Figs. 5, 6) also provide some insights into how neural activity

405 patterns change with cognitive engagement or task demands. Prior work has shown that the
406 components and network “parcels” identified through covarying activity patterns can be highly
407 similar even across different tasks (including “rest,” e.g., Laird et al., 2011; Smith et al., 2009).
408 We replicated this basic finding in that the first principal components from all four experimental
409 conditions were strikingly similar (e.g., see the leftmost columns of Figs. 5A and 6C, D). We also
410 found some small, though statistically reliable, systematic changes in the weights associated with
411 different cognitive functions across conditions (Fig. 6E). This result provided an additional way of
412 characterizing network-level differences across conditions (Fig. 4E). Taken together, these findings
413 suggest that although similar networks may be involved in different tasks, the ways in which those
414 networks are engaged may vary systematically with task demands.

415 **Concluding remarks**

416 Cognitive neuroscientists are still grappling with basic questions about the fundamental “rules”
417 describing how our brains respond, and about how brain activity patterns and the associated
418 underlying cognitive representations and computations are linked. We identified two aspects of
419 brain activity patterns, informativeness and compressibility, that appear to change systematically
420 with task demands and across brain networks. We speculate that these changes may reflect ongoing
421 tradeoffs between how robust to signal corruption versus how expressive about ongoing cognitive
422 states our brains’ activity patterns are. Our work also provides a new framework for evaluating
423 these tradeoffs in other datasets, or in future studies.

424 **Methods**

425 We measured properties of recorded neuroimaging data under different task conditions that varied
426 systematically in cognitive engagement and depth of processing. We were especially interested in
427 how *informative* and *compressible* the activity patterns were under these different conditions (Fig. 1).

428 Unless otherwise noted, all statistical tests are two-sided, all error bars and error ribbons
429 denote bootstrap-estimated 95% confidence intervals across participants, and all reported *p*-values
430 are corrected for multiple comparisons using the Benjamini-Hochberg procedure (Benjamini &
431 Hochberg, 1995).

432 **Functional neuroimaging data collected during story listening**

433 We examined an fMRI dataset collected by Simony et al. (2016) that the authors have made publicly
434 available at arks.princeton.edu/ark:/88435/dsp015d86p269k. The dataset comprises neuroimaging
435 data collected as participants listened to an audio recording of a story (intact condition; 36 par-
436 ticipants), listened to temporally scrambled recordings of the same story (17 participants in the
437 paragraph-scrambled condition listened to the paragraphs in a randomized order and 36 in the
438 word-scrambled condition listened to the words in a randomized order), or lay resting with their
439 eyes open in the scanner (rest condition; 36 participants). Full neuroimaging details may be found
440 in the original paper for which the data were collected (Simony et al., 2016). Procedures were
441 approved by the Princeton University Committee on Activities Involving Human Subjects, and by
442 the Western Institutional Review Board (Puyallup, WA). All subjects were native English speakers
443 with normal hearing and provided written informed consent. We have excerpted the relevant
444 portions of the dataset documentation here to provide information about the scanning parameters
445 and preprocessing steps used to generate the data we analyzed (the original descriptions may be
446 found at the above link):

447 Subjects were scanned in a 3T full-body MRI scanner (Skyra; Siemens) with a sixteen-
448 channel head coil. For functional scans, images were acquired using a T2* weighted
449 echo planer imaging (EPI) pulse sequence [repetition time (TR), 1500 ms; echo time (TE),
450 28 ms; flip angle, 64°], each volume comprising 27 slices of 4 mm thickness with 0 mm
451 gap; slice acquisition order was interleaved. In-plane resolution was $3 \times 3 \text{ mm}^2$ [field of
452 view (FOV), $192 \times 192 \text{ mm}^2$]. Anatomical images were acquired using a T1-weighted
453 magnetization-prepared rapid-acquisition gradient echo (MPRAGE) pulse sequence
454 (TR, 2300 ms; TE, 3.08 ms; flip angle 9°; 0.89 mm^3 resolution; FOV, 256 mm^2). To
455 minimize head movement, subjects' heads were stabilized with foam padding. Stimuli
456 were presented using the Psychophysics toolbox (Brainard, 1997; Pelli, 1997). Subjects
457 were provided with an MRI compatible in-ear mono earbuds (Sensometrics Model S14),
458 which provided the same audio input to each ear. MRI-safe passive noise-canceling
459 headphones were placed over the earbuds, for noise removal and safety.

460 Functional data were preprocessed and analyzed using FSL (www.fmrib.ox.ac.uk/fsl),

461 including correction for head motion and slice-acquisition time, spatial smoothing (6
462 mm FWHM Gaussian kernel), and high-pass temporal filtering (140 s period). Prepro-
463 cessed data were aligned to coplanar and high-resolution anatomicals and the standard
464 MNI152 brain, and interpolated to 3-mm isotropic voxels.

465 The intact and word conditions each comprised 300 TRs (7.5 minutes) per participant. The para-
466 graph condition comprised 272 TRs (6.8 minutes) per participant. The rest condition comprised
467 400 TRs (10 minutes) per participant.

468 **Hierarchical topographic factor analysis (HTFA)**

469 Following our prior related work, we used HTFA (Manning et al., 2018) to derive a compact
470 representation of the neuroimaging data. In brief, this approach approximates the timeseries
471 of voxel activations (44,415 voxels) using a much smaller number of radial basis function (RBF)
472 nodes (in this case, 700 nodes, as determined by an optimization procedure; Manning et al., 2018).
473 This provides a convenient representation for examining full-brain activity patterns and network
474 dynamics. All of the analyses we carried out on the neuroimaging dataset were performed in
475 this lower-dimensional space. In other words, each participant's data matrix was a number-of-
476 timepoints (T) by 700 matrix of HTFA-derived factor weights (where the row and column labels
477 were matched across participants). Code for carrying out HTFA on fMRI data may be found as
478 part of the BrainIAK toolbox (Capota et al., 2017; Kumar et al., 2021), which may be downloaded
479 at brainiak.org.

480 We also considered alternative approaches to obtaining compact representations of the neu-
481 roimaging data, including network parcellations (e.g., Gordon et al., 2016; Schaefer et al., 2018).
482 Whereas network parcellations are typically derived from large resting state datasets, HTFA may
483 be applied to much smaller datasets. In our prior work, we showed that HTFA applied to the same
484 dataset used here can explain full-brain activity to within a maximum of 0.25 standard deviations
485 of each voxel's observed activity in the original dataset, taken across all voxels, images, and partic-
486 ipants, using the 700-node representation we also employed here (Manning et al., 2018). Some of
487 the explanatory power of HTFA comes from the fact that each node's influence falls off smoothly
488 with distance to its center. Intuitively, the result is a representation that looks like a lightly spatially

489 smoothed version of the original data, but where the degree of smoothing varies across the brain
490 according to how spatially autocorrelated the local activity patterns are.

491 **Network permutation tests**

492 In our analyses of how informativeness varied across brain networks (Fig. 4), we considered the
493 possibility that the correlations with network order might be influenced by the numbers of nodes
494 in each network. We designed a permutation-based procedure to address this possibility, whereby
495 we repeated the above analyses using shuffled network labels. Specifically, for each of $n_1 = 10$
496 iterations, we randomly shuffled (without replacement) the network labels of the HTFA nodes, and
497 then we re-ran our entire decoding analysis pipeline, including applying PCA with $3 \dots m$ features
498 for each condition (where m is the number of nodes in the given network), and then running 100
499 cross-validation runs of the decoding procedure for each condition and number of components.
500 This resulted in 10 sets of shuffled data, where each network had the same numbers of nodes, but
501 where the decoding results no longer maintained the fidelity of each individual network.

502 We sampled the original and shuffled datasets (with replacement) to create $n_2 = 1000$ bootstrap
503 samples. For each bootstrap sample, we computed the correlations between the decoding accura-
504 cies and network order for each condition and number of components. This yielded a distribution
505 of n_2 correlation values for each condition, for both the original and shuffled datasets. We then
506 compared the distributions of Spearman's ρ values for the original and shuffled datasets using
507 two-sided independent samples Welch's t -tests.

508 **Principal components analysis (PCA)**

509 We applied group PCA (Smith et al., 2014) separately to the HTFA-derived representations of the
510 data (i.e., factor loadings) from each experimental condition. Specifically, for each condition, we
511 considered the set of all participants' T by 700 factor weight matrices. We used group PCA to project
512 these 700-dimensional matrices into a series of shared k -dimensional spaces, for $k \in \{3, 4, 5, \dots, 700\}$.
513 This yielded a set of number-of-participants matrices, each with T rows and k columns.

514 **Temporal decoding**

515 We sought to identify neural patterns that reflected participants' ongoing cognitive processing of
516 incoming stimulus information. As reviewed by Simony et al. (2016), one way of homing in on
517 these stimulus-driven neural patterns is to compare activity patterns across individuals. In partic-
518 ular, neural patterns will be similar across individuals to the extent that the neural patterns under
519 consideration are stimulus-driven, and to the extent that the corresponding cognitive representa-
520 tions are reflected in similar spatial patterns across people (Simony & Chang, 2020). Following this
521 logic, we used an across-participant temporal decoding test developed by Manning et al. (2018) to
522 assess the degree to which different neural patterns reflected ongoing stimulus-driven cognitive
523 processing across people. The approach entails using a subset of the data to train a classifier to
524 decode stimulus timepoints (i.e., moments in the story participants listened to) from neural pat-
525 terns. We use decoding (forward inference) accuracy on held-out data, from held-out participants,
526 as a proxy for the extent to which the inputted neural patterns reflected stimulus-driven cognitive
527 processing in a similar way across individuals.

528 **Forward inference and decoding accuracy**

529 We used an across-participant correlation-based classifier to decode which stimulus timepoint
530 matched each timepoint's neural pattern. For a given value of k (i.e., number of principal compo-
531 nents), we first used group PCA to project the data from each condition into a shared k -dimensional
532 space. Next, we divided the participants into two groups: a template group, $\mathcal{G}_{\text{template}}$ (i.e., training
533 data), and a to-be-decoded group, $\mathcal{G}_{\text{decode}}$ (i.e., test data). We averaged the projected data within
534 each group to obtain a single T by k matrix for each group. Next, we correlated the rows of the two
535 averaged matrices to form a T by T decoding matrix, Λ . In this way, the rows of Λ reflected time-
536 points from the template group, while the columns reflected timepoints from the to-be-decoded
537 group. We used Λ to assign temporal labels to each timepoint (row) from the test group's ma-
538 trix, using the row of the training group's matrix with which it was most highly correlated. We
539 repeated this decoding procedure, but using $\mathcal{G}_{\text{decode}}$ as the template group and $\mathcal{G}_{\text{template}}$ as the
540 to-be-decoded group. Given the true timepoint labels (for each group), we defined the decoding
541 accuracy as the average proportion of correctly decoded timepoints, across both groups (where

542 chance performance is $\frac{1}{T}$). In Figures 2 and 3 we report the decoding accuracy for each condition
543 and value of k , averaged across $n = 100$ cross validation folds.

544 **Reverse inference**

545 To help interpret the brain activity patterns we found within the contexts of other studies, we
546 created summary maps of each principal component, for each experimental condition. Each
547 principal component comprises 700 “weights” on each of the HTFA-derived RBF nodes (see
548 *Hierarchical Topographic Factor Analysis*). For each node, we evaluated its RBF at the locations of
549 every voxel in the standard 2 mm MNI152 template brain and multiplied the RBF by the node’s
550 weight. The sum of these weighted RBF activation maps provides a full-brain image, in MNI152
551 space, of the given principal component (Fig. S4).

552 Next, we considered 80 topics estimated using Latent Dirichlet Allocation (Blei et al., 2003)
553 applied to 9,204 functional neuroimaging articles in the Neurosynth database (Rubin et al., 2017).
554 The topics, as well as associated brain maps identified using Neurosynth, were identified and
555 reported in several prior studies (Chen et al., 2020; Fox et al., 2014; Sul et al., 2017). The topic
556 labels for each topic were generated automatically with the following ChatGPT (OpenAI, 2023)
557 prompt: “Please help me come up with intuitive labels for topics I found by fitting a topic model
558 to thousands of neuroscience and psychology articles. I’ll paste in the top 10 highest-weighted
559 words for each topic, and I’d like you to respond with a suggested label. For each topic, please
560 respond with just the topic label and no other formatting or text. Here are the next topic’s top
561 words:” followed by a comma-separated list of the given topic’s top-weighted words reflected
562 in the Table S1. For some topics, ChatGPT responded with a longer-form response rather than a
563 concise topic label. In these instances, on a case-by-case basis, we used a second follow-up prompt
564 to achieve the given topic’s label: “Could you please come up with a more concise label for that
565 topic?”. We then manually identified a set of 11 cognitive labels that were intended to encapsulate
566 a representative range of widely studied low-level and high-level cognitive functions. In choosing
567 the set of cognitive labels, we jointly considered each topic’s ChatGPT-derived topic label, along
568 with the top-weighted words for the topic. We attempted to generate a concise set of labels that
569 still spanned the full set of cognitive functions reflected across the 80 topics. Topics that appeared

570 unrelated to specific cognitive functions (e.g., topics related to specific methods or clinical themes)
571 are designated with dashes in Table S1.

572 Finally, following an approach used in several prior studies (Chen et al., 2020; Fox et al., 2014;
573 Sul et al., 2017) we treated the correlation between a given component's brain map and each topic's
574 brain map as an approximate measure of how much the component was reflective of the given
575 topic. This resulted in a set of 80 "weights" (correlation coefficients) for each component's brain
576 map, with one weight per Neurosynth-derived topic.

577 Ranking cognitive processes

578 We manually identified 11 cognitive labels spanning the set of 80 Neurosynth-derived topics:
579 cognitive control, language processing, memory, emotion, social cognition, spatial cognition, at-
580 tention, reward, sensory perception, motor control, and resting state. We then used ChatGPT
581 to automatically "rank" the processes from high-level to low-level using the following prompt:
582 "Please rank these cognitive processes from highest-level to lowest-level, where higher values
583 indicate higher-order or higher-level processes. Return the result as a csv file with a header row
584 and two columns: 'Cognitive label' and 'Rank'. Here are the processes: cognitive control, lan-
585 guage processing, memory, emotion, social cognition, spatial cognition, attention, reward, sensory
586 perception, motor control, resting state". Table S2 displays the output.

587 We recognize that ChatGPT is not omniscient, nor should it be treated as an expert cognitive
588 neuroscientist. We therefore reviewed ChatGPT's responses carefully by hand to verify that they
589 seemed reasonable to us. Whereas prior work has often constructed such rankings by hand, we see
590 our use of ChatGPT in this case as a small additional "sanity check" on our rankings that helped
591 us to be slightly more objective than if we had simply created the rankings ourselves manually.

592 In the analysis presented in Figure 6E, we summarize difference in topic weightings across
593 experimental conditions. In particular, we sought to characterize how the dominant neural patterns
594 evoked by each experimental condition weighted on different cognitive functions. For each of the
595 top five principal components from each experimental condition (Fig. 5), we computed the average
596 weights for each of the 11 manually identified (and ChatGPT-ranked) cognitive labels described
597 above (Tab. S2). We then fit a line separately for each experiment condition (x -values: cognitive

rank; y -values: weights). In carrying out this analysis, we used a bootstrap procedure to estimate the variability in the slopes of the regression lines, whereby we repeated this process for each of $n = 100$ iterations, each time resampling (with replacement) the set of observed ranks and weights. This procedure yielded distributions of 100 estimated slopes for each experimental condition. We used these distributions to compare the slopes across experimental conditions and to estimate 95% confidence intervals.

604 Synthetic data

To help illustrate the relationship between informativeness and compressibility (Fig. 1), we generated four synthetic datasets, varying in informativeness and compressibility. Each dataset comprised simulated observations of $K = 25$ features across $N = 100$ timepoints, from each of $S = 10$ participants. To create each dataset, we first constructed a “template” matrix of N timepoints by K features. We then generated participant-specific data by adding independent noise to each entry in template matrix, drawn from the unit normal distribution (i.e., with a mean of 0 and a variance of 1). We repeated this process for each participant, yielding S participant-specific matrices for each dataset.

Since we estimate informativeness using the temporal decoding accuracy across participants, highly informative data will tend to have observations that are highly timepoint specific. Relatively uninformative data, in contrast, will tend to have more similar observations across timepoints. To generate data with “high informativeness,” we constructed template matrices whose rows (observations) were drawn independently from zero-mean multivariate normal distributions. The covariances of these distributions were determined according to the desired compressibility of the data, as described below. We used a multi-step process to generate data with “low informativeness.” First we generated new template matrices using the same procedure as for the “high informativeness” datasets. We then multiplied each matrix by a constant ($\rho = 0.1$) and computed the cumulative sum of each matrix’s rows. This yielded matrices whose rows were highly similar across observations.

Compressibility reflects the extent to which decoding accuracy is affected by reducing the number of components used to represent the data. Highly compressible data will tend to exhibit more

626 similarities across features, whereas less compressible data will tend to show greater independence
627 across features. To generate data with “high compressibility,” we set the covariance matrix of the
628 multivariate normal distribution to a toeplitz matrix whose first row was given by $[K, K - 1, \dots, 1]$.
629 To generate data with “low compressibility,” we set the covariance matrix to the identity matrix.

630 Template matrices for datasets with high informativeness and high compressibility, high in-
631 formativeness and low compressibility, low informativeness and high compressibility, and low
632 informativeness and low compressibility are displayed in Figure 1C. The corresponding decoding
633 curves are displayed in Figure 1D.

634 **Data and code availability**

635 All of the code used to produce the figures and results in this manuscript, along with links to the
636 corresponding data, may be found at github.com/ContextLab/pca_paper.

637 **Acknowledgements**

638 We acknowledge discussions with Rick Betzel, Luke Chang, Emily Finn, and Jim Haxby. Our
639 work was supported in part by NSF CAREER Award Number 2145172 to J.R.M. The content is
640 solely the responsibility of the authors and does not necessarily represent the official views of our
641 supporting organizations. The funders had no role in study design, data collection and analysis,
642 decision to publish, or preparation of the manuscript.

643 **Author contributions**

644 Conceptualization: J.R.M. and L.L.W.O. Methodology: J.R.M. and L.L.W.O. Implementation:
645 J.R.M. and L.L.W.O. Analysis: J.R.M. and L.L.W.O. Writing, Reviewing, and Editing: J.R.M. and
646 L.L.W.O. Funding acquisition: J.R.M. Supervision: J.R.M.

647 **References**

- 648 Adachi, Y., Osada, T., Sporns, O., Watanabe, T., Matsui, T., Miyamoto, K., & Miyashita, Y.
649 (2012). Functional connectivity between anatomically unconnected areas is shaped by collective
650 network-level effects in the macaque cortex. *Cerebral Cortex*, 22(7), 1586–1592.
- 651 Alvarez, S. A. (2002). *An exact analytical relation among recall, precision, and classification accuracy in*
652 *information retrieval* (Technical Report No. BCCS-02-01). Boston College.
- 653 Baldassano, C., Chen, J., Zadbood, A., Pillow, J. W., Hasson, U., & Norman, K. A. (2017). Discov-
654 ering event structure in continuous narrative perception and memory. *Neuron*, 95(3), 709–721.
- 655 Bassett, D. S., & Sporns, O. (2017). Network neuroscience. *Nature Neuroscience*, 20(3), 353–364.
- 656 Benjamini, Y., & Hochberg, Y. (1995). Controlling the False Discovery Rate: a practical and
657 powerful approach to multiple testing. *Journal of Royal Statistical Society, Series B*, 57, 289–300.
- 658 Blei, D. M., Ng, A. Y., & Jordan, M. I. (2003). Latent dirichlet allocation. *Journal of Machine Learning*
659 *Research*, 3, 993–1022.
- 660 Brainard, D. H. (1997). The psychophysics toolbox. *Spatial Vision*, 10, 443–446.
- 661 Brovelli, A., Ding, M., Ledberg, A., Chen, Y., Nakamura, R., & Bressler, S. (2004). Beta oscillations in
662 a large-scale sensorimotor cortical network: directional influences revealed by Granger causality.
663 *Proceedings of the National Academy of Sciences, USA*, 101(26), 9849–9854.
- 664 Bullmore, E., & Sporns, O. (2009). Complex brain networks: graph theoretical analysis of structural
665 and functional systems. *Nature Reviews Neuroscience*, 10(3), 186–198.
- 666 Capota, M., Turek, J., Chen, P.-H., Zhu, X., Manning, J. R., Sundaram, N., ... Shin, Y. S. (2017).
667 *Brain imaging analysis kit*.
- 668 Chang, L. J., Jolly, E., Cheong, J. H., Rapuano, K., Greenstein, N., Chen, P.-H. A., & Manning, J. R.
669 (2021). Endogenous variation in ventromedial prefrontal cortex state dynamics during naturalis-
670 tic viewing reflects affective experience. *Science Advances*, 7(17), doi.org/10.1126/sciadv.abf7129.

- 671 Chen, P.-H. A., Jolly, E., Cheong, J. H., & Chang, L. J. (2020). Intersubject representational
672 similarity analysis reveals individual variations in affective experience when watching erotic
673 movies. *NeuroImage*, 216(116851), doi.org/10.1016/j.neuroimage.2020.116851.
- 674 Cole, M. W., Bassett, D. S., Power, J. D., Braver, T. S., & Petersen, S. E. (2014). Intrinsic and
675 task-evoked network architectures of the human brain. *Neuron*, 83(1), 238–251.
- 676 Dhamala, M., Rangarajan, G., & Ding, M. (2008). Analyzing information flow in brain networks
677 with nonparametric Granger causality. *NeuroImage*, 41(2), 354–362.
- 678 Finn, E. S., Scheinost, D., Finn, D. M., Shen, X., Papademetris, X., & Constable, R. T. (2017).
679 Can brain state be manipulated to emphasize individual differences in functional connectivity.
680 *NeuroImage*, 160, 140–151.
- 681 Finn, E. S., Shen, X., Scheinost, D., Rosenberg, M. D., Huang, J., Chun, M. M., ... Constable, R. T.
682 (2015). Functional connectome fingerprinting: identifying individuals using patterns of brain
683 connectivity. *Nature Neuroscience*, 18, 1664–1671.
- 684 Fox, A. S., Chang, L. J., Gorgolewski, K. J., & Yarkoni, T. (2014). Bridging psychology and
685 genetics using large-scale spatial analysis of neuroimaging and neurogenetic data. *bioRxiv*,
686 doi.org/10.1101/012310.
- 687 Glerean, E., Salmi, J., Lahnakoski, J. M., Jääskeläinen, I. P., & Sams, M. (2012). Functional magnetic
688 resonance imaging phase synchronization as a measure of dynamic functional connectivity.
689 *Brain Connectivity*, 2(2), 91–101.
- 690 Gordon, E. M., Laumann, T. O., Adeyemo, B., Huckins, J. F., Kelley, W. M., & Petersen, S. E. (2016).
691 Generation and evaluation of a cortical area parcellation from resting-state correlations. *Cerebral
692 Cortex*, 26, 288–303.
- 693 Gratton, C., Laumann, T. O., Nielsen, A. N., Greene, D. J., Gordon, E. M., Gilmore, A. W., ...
694 Petersen, S. E. (2018). Functional brain networks are dominated by stable group and individual
695 factors, not cognitive or daily variation. *Neuron*, 98(2), 439–452.
- 696 Hasson, U., Yang, E., Vallines, I., Heeger, D. J., & Rubin, N. (2008). A hierarchy of temporal
697 receptive windows in human cortex. *The Journal of Neuroscience*, 28(10), 2539–2550.

- 698 Korzeniewska, A., Crainiceanu, C. M., Kus, R., Franaszczuk, P. J., & Crone, N. E. (2008). Dynamics
699 of event-related causality in brain electrical activity. *Human Brain Mapping*, 29(10).
- 700 Kumar, M., Anderson, M. J., Antony, J. W., Baldassano, C., Brooks, P. P., Cai, M. B., ... Norman,
701 K. A. (2021). BrainIAK: the brain image analysis kit. *Aperture*, doi.org/10.52294/31bb5b68-2184-
702 411b-8c00-a1dacb61e1da.
- 703 Laird, A. R., Fox, P. M., Eickhoff, S. B., Turner, J. A., Ray, K. L., McKay, D. R., ... Fox, P. T. (2011).
704 Behavioral interpretations of intrinsic connectivity networks. *Journal of Cognitive Neuroscience*,
705 23(12), 4022–4037.
- 706 Lerner, Y., Honey, C. J., Silbert, L. J., & Hasson, U. (2011). Topographic mapping of a hierarchy of
707 temporal receptive windows using a narrated story. *The Journal of Neuroscience*, 31(8), 2906–2915.
- 708 Lynn, C. W., & Bassett, D. S. (2021). Quantifying the compressibility of complex networks.
709 *Proceedings of the National Academy of Sciences, USA*, 118(32), e2023473118.
- 710 Mack, M. L., Preston, A. R., & Love, B. C. (2020). Ventromedial prefrontal cortex compression
711 during concept learning. *Nature Communications*, 11(46), doi.org/10.1038/s41467-019-13930-8.
- 712 Manning, J. R. (2023). Context reinstatement. In M. J. Kahana & A. D. Wagner (Eds.), *Handbook of
713 human memory*. Oxford University Press.
- 714 Manning, J. R., Zhu, X., Willke, T. L., Ranganath, R., Stachenfeld, K., Hasson, U., ... Norman,
715 K. A. (2018). A probabilistic approach to discovering dynamic full-brain functional connectivity
716 patterns. *NeuroImage*, 180, 243–252.
- 717 Norman, K. A., Polyn, S. M., Detre, G. J., & Haxby, J. V. (2006). Beyond mind-reading: multi-voxel
718 pattern analysis of fMRI data. *Trends in Cognitive Sciences*, 10(9), 424–430.
- 719 OpenAI. (2023). ChatGPT. <https://chat.openai.com>.
- 720 Owen, L. L. W., Chang, T. H., & Manning, J. R. (2021). High-level cognition during story listening is
721 reflected in high-order dynamic correlations in neural activity patterns. *Nature Communications*,
722 12(5728), doi.org/10.1038/s41467-021-25876-x.

- 723 Owen, L. L. W., Muntianu, T. A., Heusser, A. C., Daly, P., Scangos, K. W., & Manning, J. R. (2020). A
724 Gaussian process model of human electrocorticographic data. *Cerebral Cortex*, 30(10), 5333–5345.
- 725 Pelli, D. G. (1997). The VideoToolbox software for visual psychophysics: transforming numbers
726 into movies. *Spatial Vision*, 10, 437–442.
- 727 Preti, M. G., Bolton, T. A. W., & Van De Ville, D. (2017). The dynamic functional connectome:
728 state-of-the-art and perspectives. *NeuroImage*, 160, 41–54.
- 729 Regev, M., Simony, E., Lee, K., Tan, K. M., Chen, J., & Hasson, U. (2018). Propagation of information
730 along the cortical hierarchy as a function of attention while reading and listening to stories.
731 *Cerebral Cortex*.
- 732 Rogers, B. P., Morgan, V. L., Newton, A. T., & Gore, J. C. (2007). Assessing functional connectivity
733 in the human brain by fMRI. *Magnetic Resonance Imaging*, 25(11), 1347–1357.
- 734 Rubin, T. N., Kyoejo, O., Gorgolewski, K. J., Jones, M. N., Poldrack, R. A., & Yarkoni, T. (2017).
735 Decoding brain activity using a large-scale probabilistic functional-anatomical atlas of human
736 cognition. *PLoS Computational Biology*, 13(10), e1005649.
- 737 Rubinov, M., & Sporns, O. (2010). Complex network measures of brain connectivity: uses and
738 interpretations. *NeuroImage*, 52, 1059–1069.
- 739 Scangos, K. W., Khambhati, A. N., Daly, P. M., Owen, L. L. W., Manning, J. R., Ambrose, J. B.,
740 ... Chang, E. F. (2021). Biomarkers of depression symptoms defined by direct intracranial
741 neurophysiology. *Frontiers in Human Neuroscience*, 15, doi.org/10.3389/fnhum.2021.746499.
- 742 Schaefer, A., Kong, R., Gordon, E. M., Laumann, T. O., Z, X.-N., Holmes, A. J., ... Yeo, B. T. T. (2018).
743 Local-global parcellation of the human cerebral cortex from intrinsic functional connectivity MRI.
744 *Cerebral Cortex*, 28, 3095–3114.
- 745 Shannon, C. E. (1948). A mathematical theory of communication. *Bell System Technical Journal*,
746 27(3), 379–423.
- 747 Simony, E., & Chang, C. (2020). Analysis of stimulus-induced brain dynamics during naturalistic
748 paradigms. *NeuroImage*, 216, 116461.

- 749 Simony, E., Honey, C. J., Chen, J., & Hasson, U. (2016). Dynamic reconfiguration of the default
750 mode network during narrative comprehension. *Nature Communications*, 7(12141), 1–13.
- 751 Sizemore, A. E., Giusti, C., Kahn, A., Vettel, J. M., Betzel, R. F., & Bassett, D. S. (2018). Cliques and
752 cavities in the human connectome. *Journal of Computational Neuroscience*, 44(1), 115–145.
- 753 Smith, S. M., Beckmann, C. F., Andersson, J., Auerbach, E. J., Bijsterbosch, J., Douaud, G., ...
754 Glasser, M. F. (2013). Resting-state fMRI in the Human Connectome Project. *NeuroImage*, 80,
755 144–168.
- 756 Smith, S. M., Fox, P. T., Miller, K. L., Glahn, D. C., Fox, P. M., Mackay, C. E., ... Beckmann,
757 C. F. (2009). Correspondence of the brain's functional architecture during activation and rest.
758 *Proceedings of the National Academy of Sciences, USA*, 106(31), 13040–13045.
- 759 Smith, S. M., Hyvärinen, A., Varoquaux, G., Miller, K. L., & Beckmann, C. F. (2014). Group-PCA
760 for very large fMRI datasets. *NeuroImage*, 101, 738–749.
- 761 Smith, S. M., Vidaurre, D., Beckmann, C. F., Glasser, M. F., Jenkinson, M., Miller, K. L., ... Van
762 Essen, D. C. (2013). Functional connectomics from resting-state fMRI. *Trends in Cognitive Sciences*,
763 17(12), 666–682.
- 764 Sporns, O., & Betzel, R. F. (2016). Modular brain networks. *Annual Review of Psychology*, 67,
765 613–640.
- 766 Sporns, O., & Honey, C. J. (2006). Small worlds inside big brains. *Proceedings of the National Academy
767 of Sciences, USA*, 103(51), 19219–19220.
- 768 Sporns, O., & Zwi, J. D. (2004). The small world of the cerebral cortex. *Neuroinformatics*, 2(2),
769 145–162.
- 770 Srinivasan, R., Winter, W. R., Ding, J., & Nunez, P. L. (2007). EEG and MEG coherence: Measures of
771 functional connectivity at distinct spatial scales of neocortical dynamics. *Journal of Neuroscience
772 Methods*, 166, 41–52.

- 773 Sul, S., Güroğlu, B., Crone, E. A., & Chang, L. J. (2017). Medial prefrontal cortical thinning
774 mediates shifts in other-regarding preferences during adolescence. *Scientific Reports*, 7(8510),
775 doi.org/10.1038/s41598-017-08692-6.
- 776 Tomasi, D., & Volkow, N. D. (2011). Association between functional connectivity hubs and brain
777 networks. *Cerebral Cortex*, 21, 2003–2013.
- 778 Yeo, B. T. T., Krienen, F. M., Sepulcre, J., Sabuncu, M. R., Lashkari, D., Hollinshead, M., . . . Buckner,
779 R. L. (2011). The organization of the human cerebral cortex estimated by intrinsic functional
780 connectivity. *Journal of Neurophysiology*, 106(3), 1125–1165.